OPEN ACCESS
Journal of Multidisciplinary Applied Natural Science Vol. xx No. xx (xxxx) https://doi.org/10.47352/jmans.2774-3047.471
Check for updates
Research Article

New Limonoid from *Chisocheton macrophyllus*: Isolation, Synthesis, Molecular Docking Studies, and Cytotoxicity against Cancer Cells

Muhammad Badrul Huda, Nurlelasari Nurlelasari*, Faris Hermawan, Wahyu Safriansyah, Unang Supratman, and Yudha Prawira Budiman

Received : December 20, 2025	Revised : April 17, 2026	Accepted : June 22, 2026	Online : July 31, 2026

Abstract
Dysobinin is a naturally occurring limonoid and a type of triterpenoid, which shows certain efficacy, although its prospects in the field of pharmacology are still limited. Therefore, this study aimed to improve the pharmacological properties of dysobinin through structural rearrangement. A 56% yield was obtained using Selectfluor to convert dysobinin into a novel molecule, specifically 22α-carboxyacid-dysobinin (**5**). Compared to the other compounds, 22α-carboxyacid-dysobinin (**5**) exhibited significantly higher cytotoxicity against human epithelial tumor (HeLa) and B16-F10 cancer cells. However, this compound **5** exhibited the lowest cytotoxicity against MCF-7 cancer cells. Subsequently, a docking study showed that compound **5** had binding energies of -9.61, -7.81, and -6.08 kcal/mol for EGFR, Bcl-2, and Tyrosinase, respectively. In the prediction of pharmacokinetic parameters, compound **5** fulfilled the minimum standard parameters for the ADMET properties. Therefore, compound **5** may be considered a promising lead compound for anticancer development, warranting further optimization and validation.

Keywords: B16-F10, HeLa, MCF-7, molecular docking, selectfluor

1. INTRODUCTION

Cancer is the second leading cause of mortality, after cardiovascular diseases. In 2023, over 19.5 million new cancer cases and approximately 10.4 million cancer-related fatalities were reported [1]. In 2022, Indonesia recorded approximately 408,000 new cancer cases and more than 242,000 cancer-related deaths, indicating a substantial and growing public health concern in the country [2]. Cancer is a broad term that includes numerous types of malignant tumors. Uncontrolled cell development, aberrant cell migration, and unintended dissemination of adjacent tissues and organs are characteristic features of these tumors [3][4]. Cancer development is driven by multiple factors, including genetic mutations, environmental exposures, lifestyle factors, and infections, which disrupt cellular signaling, regulatory mechanisms, and apoptotic pathways, leading to the transformation of normal cells into cancer cells, characterized by uncontrolled proliferation [5]. Chemotherapy is one of the most widely used cancer treatment methods owing to its broad application across various cancer types. However, chemotherapy has certain limitations, including drug resistance, selectivity, efficiency, and adverse effects [6]. Identifying new anticancer agents that exhibit greater selectivity for cancer cells and result in fewer adverse effects, such as myelosuppression, gastrointestinal toxicity, alopecia, immunosuppression, and organ toxicity, is essential to address these challenges. Therefore, research on the discovery of bioactive compounds as anticancer agents with improved inhibitory activity needs to be further developed.

The discovery of new drug candidates with high cytotoxicity can be achieved by modifying natural compounds. Several studies have shown that limonoids isolated from *Chisocheton macrophyllus* exhibit anticancer activity [7]-[10]. However, the activity of limonoid dysobinin remains relatively low. This is likely due to the absence of specific functional groups that effectively inhibit cancer cell growth. Nevertheless, these limonoid compounds have the potential to serve as model compounds for the development of breast cancer agents, as they possess relatively high mass among plant-derived isolates [11]. This characteristic meets one of the

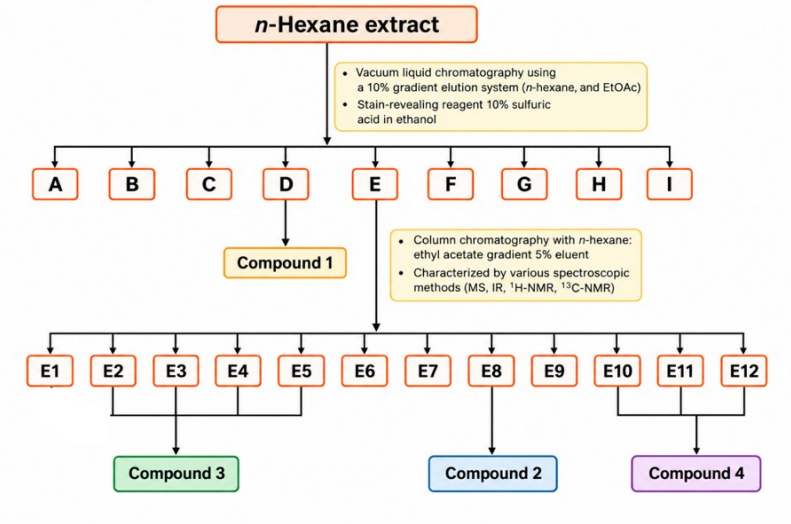

Figure 1. Diagram isolation of compounds from *C. macrophyllus* seeds.

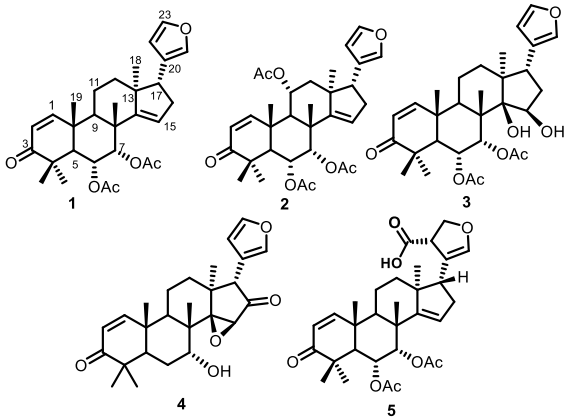

Figure 2. Structures of Compounds **1-5**.

key requirements for structural modification or development aimed at enhancing their activity via functional group transformation.

In silico molecular docking studies are essential for predicting ligand–protein interactions and binding stability [12]. Among the key anticancer targets, Epidermal Growth Factor Receptor (EGFR) promotes proliferation, angiogenesis, and metastasis and suppresses apoptosis [13], with elevated expression reported in MCF-7 cells [14]. B-cell lymphoma 2 (Bcl-2) regulates cell survival by inhibiting pro-apoptotic pathways and is stably expressed in HeLa cells [15][16]. Tyrosinase, a key enzyme in melanogenesis, catalyzes the conversion of L-tyrosine to melanin via sequential oxidation reactions [17]-[20]. In addition to pigmentation, tyrosinase is closely associated with melanoma progression and cellular defense mechanisms. This is particularly relevant in melanoma models, such as B16-F10, which exhibit high melanogenic activity and are widely used to evaluate antimelanoma agents. This study shows that molecular docking analyses of proteins can predict the inhibitory mechanism of the tested compound at the active site of the protein. This is the first study to report the rearrangement of dysobinin using this method. One synthesized molecule and four extracted compounds were tested for their inhibitory effects on MCF-7, HeLa, and B16-F10 cancer cells, and molecular docking was used to explore the underlying mechanisms.

2. MATERIALS AND METHODS

2.1. Instruments and Chemicals

The Instruments used in this study consisted of an ultraviolet (UV) spectrum measured using a TECAN Infinite M200 Pro spectrophotometer with methanol as the solvent. Optical rotations were recorded using a Perkin Elmer 341 polarimeter

(Waltham, MA, USA). Infrared (IR) spectra were obtained using a PerkinElmer Spectrum-100 FTIR spectrometer. Mass spectra were obtained using a Waters Xevo QTOF-HR-MS instrument. ^{1}H and ^{13}C NMR spectra were obtained on a Bruker Ascend spectrometer at 700 MHz for ^{1}H and 175 MHz for ^{13}C, using TMS as the internal standard. Separation and purification were carried out using silica gel 60 (Merck, 70–230 and 230–400 mesh). Thin-layer chromatography (TLC) was performed on GF_{254} silica gel plates (Merck, 0.25 mm thickness), and visualization was performed under UV-visible light at 254 and 365 nm. For limonoid detection, Erlich's reagent (*p*-dimethylaminobenzaldehyde) diluted in ethanol (10% H_2SO_4) was sprayed onto the plate and heated.

The materials used for isolation consisted of *C. macrophyllus* seeds, technical organic solvents (re-distilled), and pro-analysts such as methanol, *n*-hexane, ethyl acetate, chloroform, acetone, and other organic solvents, silica gel GF_{254} for thin-layer chromatography, silica gel G_{60} for vacuum liquid chromatography, silica gel 70-230 mesh, and silica gel 200-400 mesh for column chromatography, and TLC plates. The staining reagent was 10% sulfuric acid in ethanol. *Chisocheton macrophyllus* seeds were collected from the Bogor Botanical Garden in West Java Province, Indonesia. The Herbarium Bogoriense in Bogor houses a voucher specimen (No. Bo-1295453). The chemicals required for the synthesis included acetonitrile, methanol, aquadest, Selectfluor, and dysobinin. The materials required for testing the cytotoxic activity of the isolates included PrestoBlue reagent, B16-F10, HeLa, and MCF-7 breast cancer cells, RPMI 1640 medium culture media, 10% Fetal Bovine Serum (FBS), trypsin-EDTA, dimethyl sulfoxide (DMSO), and doxorubicin as a positive control.

2.2. Extraction and Isolation

Dry seeds of *C. macrophyllus* (3.5 kg) were macerated in methanol for 6 × 24 h and then evaporated to yield 414.0 g of the crude extract. The crude extract was partitioned using *n*-hexane, ethyl acetate, and *n*-butanol, yielding 197.0, 41.7, and 15.0 g of concentrated extracts, respectively, for each solvent. The *n*-hexane extract was further separated by vacuum liquid chromatography (VLC) using a gradient elution system (*n*-hexane, ethyl acetate (EtOAc), and methanol (MeOH) on silica gel G_{60}, producing nine fractions (A-I). Fraction D (5 g) was purified by recrystallization to obtain compound **1** (500 mg). Fraction E (2.04 g) was chromatographed using a gradient mixture (2.5% ethyl acetate in *n*-hexane) on silica gel (70-230 mesh). Subfraction E9 (289.4 mg) was further purified by recrystallization from chloroform to obtain compound **2** (200 mg). Subfractions E2–E5 (142.5 mg) were combined and separated using a silica gel column to obtain compound **3** (16.1 mg). Compound **4** (18.0 mg) was isolated by purifying subfractions E10–E12 (96 mg) using a silica gel column chromatography (Figure 1).

2.3. Procedure for Selectfluor

A Schlenk flask was filled with acetonitrile (2.0 mL), methanol (2.0 mL), aquadest (0.2 mL), Selectfluor (0.25 mmol), and dysobinin (0.25 mmol) in an inert environment (Figure 2). The resulting mixture was stirred and sealed for 20-h at room temperature. Chromatography was performed on a silica gel column using *n*-hexane: EtOAc (8:2) as the eluent. This process yielded compound **5** (72 mg, 56%) [21].

2.5. Cytotoxic Activity

The PrestoBlue® test was used to assess the cytotoxicity of compounds **1**–**5** by conducting a cell viability test. The cells were cultured in Roswell

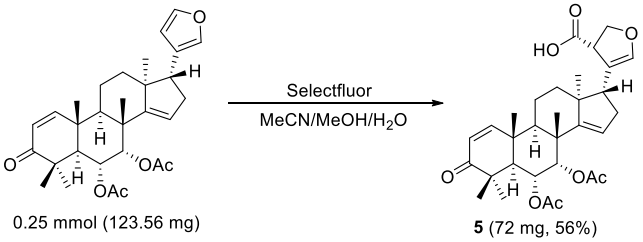

Figure 3. Reaction of rearranged Dysobinin.

Table 1. Comparison data between 22*α*-carboxyacid-dysobinin (**5**) with dysobinin (**1**).

C	Dysobinin		22*α*-carboxyacid-dysobinin	
	^{1}H-NMR (500 MHz)	^{13}C-NMR (125 MHz)	^{1}H-NMR (700 MHz)	^{13}C-NMR (175 MHz)
	δ_H ppm (ΣH; mult; *J*=Hz)	δ_C ppm	δ_H ppm (ΣH; mult; *J*=Hz)	δ_C ppm
1	7.30 (1H; d; 10.3)	158.2	7.16 (1H; d; 10.1)	157.3
2	5.84 (1H; d; 10.3)	126.6	5.94 (1H; d; 10.3)	126.1
3	-	204.1	-	204.6
4	-	45.6	-	44.9
5	2.50 (1H; m)	48.9	2.54 (1H; m, 11.5)	47.9
6	5.40 (1H; m)	70.0	5.47 (1H; m)	70.2
7	5.40 (1H; d)	75.1	5.42 (1H; m)	74.6
8	-	43.9	-	43.1
9	1.28 (1H; m)	38.3	2.25 (1H; m)	37.0
10	-	41.6	-	40.8
11	1.80 (1H; m)	17.0	1.78 (1H; m)	16.4
12	2.30 (1H; m); 2.50 (1H; m)	35.3	2.07 (2H; t)	32.6
13	-	47.9	-	47.3
14	-	159.7	-	158.1
15	5.40 (1H; m)	120.2	5.38 (1H; m)	119.2
16	1.73 (1H; m); 1.93 (1H; m)	33.6	2.50 (2H; td; 11.6, 6.9)	34.0
17	2.84 (1H; dd; 7.4; 11.3)	52.7	2.83 (1H; dd; 10.9, 7.3)	50.9
18	1.35 (3H; s)	27.1	1.34 (3H; s)	26.9
19	1.22 (3H; s)	32.1	1.25 (3H; s)	31.7
20	-	125.5	-	134.1
21	7.40 (1H; s)	140.9	7.23 (1H; s)	146.6
22	6.40 (1H; d)	112.0	4.85 (1H; d; 2.6)	69.9
23	7.50 (1H; d)	143.7	2.80 (1H; d; 1.8)	50.7
28	1.15 (3H; s)	20.7	1.17 (3H; s)	20.5
29	1.22 (3H; s)	20.9	1.19 (3H; s)	20.8
30	1.22 (3H; s)	21.2	0.85 (3H; s)	21.0
1'	2.00 (3H; s)	21.3	1.99 (3H; s)	21.1
2'	-	170.6	-	170.1
1"	2.00 (3H; s)	22.4	2.01 (3H; s)	21.4
2"	-	170.6	-	170.3
1'"			-	174.2

Park Memorial Institute (RPMI) medium supplemented with 10% (v/v) FBS and 1µL/mL antibiotics. The cultures were then maintained at 37°C in a humid environment with 5% CO_2. MCF-7, HeLa, B-16-F10, and CV-1 cells were seeded into 96-well culture plates at a density of 1.7×10^4 cells per well. After a 24-h incubation period, the old media were replaced with fresh media containing different samples at various concentrations (7.81, 15.63, 31.25, 62.5, 125, 250, 500, and 1000 µg/mL) and a control. The samples and cells were cultured for 24-h prior to the addition of PrestoBlue® reagent (resazurin dye) to the wells. The data were subsequently assessed using a multimode reader at 570 nm. Finally, the IC_{50} values, which indicate the concentration of chemicals that caused a 50% decrease in cell viability, were calculated using the linear regression method in Microsoft Excel. In this particular setting, the absorbance observed in the control wells directly indicated a cell viability of 100% [22].

2.6. Molecular Docking

The crystal structures of the EGFR, Bcl-2, and Tyrosinase protein complexes and their ligands were downloaded from the Protein Data Bank (https://www.rcsb.org/) using PDB IDs 4HJO, 2W3L, and 2Y9X, respectively. Furthermore, the ligand and protein structures were separated using Chimera software and saved in PDB format [23]. All tested compounds were constructed in a three-dimensional structure using Avogadro software [24]. Subsequently, the structures of these compounds were optimized using Orca software with the DFT B3LYP 3-21G method, and the output files were generated in PDB format [25]. All compounds were docked using AutoDock4. The docking grid was defined as 40 × 40 × 40 grid points with a grid spacing of 0.375 Å and was centered on the binding site occupied by the native ligand. The Lamarckian Genetic Algorithm (LGA)

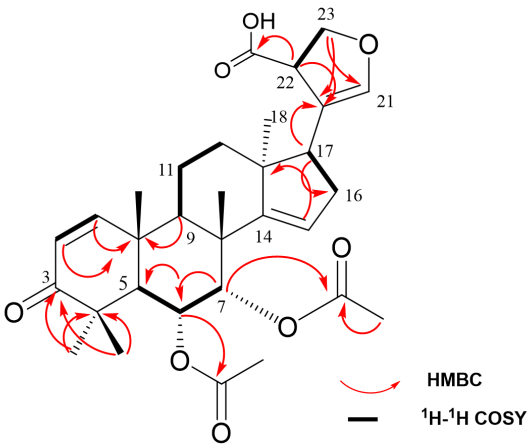

Figure 4. Selected HMBC and ^{1}H-^{1}H COSY correlations for compound **5**.

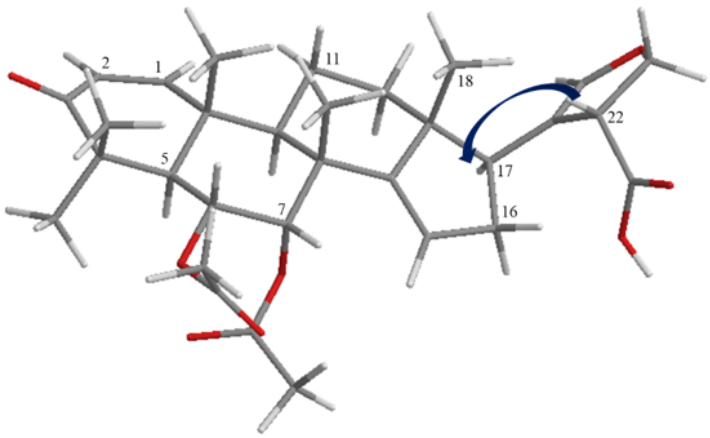

Figure 5. Selected ^{1}H-^{1}H NOESY correlations of compound **5**.

Table 2. Cytotoxicity of compounds **1**–**5** in MCF-7, HeLa, B16-F10, and CV-1 cancer cells.

Compound	IC_{50} (µg/mL)			
	MCF-7	HeLa	B16-F10	CV-1
Dysobinin (**1**)	66.7	60.0	71.52	>250.00
11α-acetoxydysobinin (**2**)	>250	>250	>250.00	>250.00
Dysobinol (**3**)	96.2	>250	40.26	>250.00
7-deacetylepoxyazadiradione (**4**)	243.7	237.14	>250.00	>250.00
22α-carboxyacid-dysobinin (**5**)	>300	18.30	23.84	177.10
Doxorubicin	43.18	16.24	51.85	39.48

was used for 50 runs. The interactions between the ligand and protein were visualized using Biovia Discovery Studio 2019.

The 3D structure of compound **5** was converted into the SMILES format using Biovia Discovery Studio 2019 software and uploaded one by one to the pkCSM website [26]. Physicochemical and ADMET parameters were determined using the ADMET menu. Furthermore, pkCSM provides data on Lipinski's rule of five: adsorption, distribution, metabolism, excretion, and toxicity.

3. RESULTS AND DISCUSSIONS

3.1. Structure Elucidation

The *n*-hexane extract of *C. macrophyllus* seeds yielded compounds **1**–**4** (Figure 2). The NMR data for compounds **1**–**4** were compared with reference data to identify their molecular structures. Based on this comparison, compounds **1**–**4** were identified as dysobinin (**1**), 11α-acetoxydysobinin (**2**), dysobinol (**3**), and 7-deacetylepoxyazadiradione (**4**), which are well-known chemical compounds [27].

The synthesis of dysobinin analogs using Selectfluor was performed following the method reported by Isabelle et al. [28]. The reaction was performed in a mixed solvent system of MeCN/MeOH/H_2O, which also functioned as a nucleophilic medium. This process afforded compound **5** with a 56% yield. The reaction mechanism is initiated by the opening of the furan ring, triggered by the electrophilic activation of the furan moiety by Selectfluor, which acts as both a source of electrophilic fluorine (F^+) and an oxidizing agent. Owing to its highly π-electron-rich nature, the furan ring undergoes an initial attack by F^+ at the α-position, generating a highly reactive dearomatized radical cation intermediate [29][30]. This unstable intermediate is rapidly trapped by methanol in the MeCN/MeOH/H_2O solvent system, leading to the formation of an alkoxy species. This intermediate subsequently undergoes stepwise ring opening of furan through cleavage of the C–O bond. In the subsequent stage, the presence of water facilitates further hydrolysis and oxidative rearrangement, ultimately yielding a more stable carboxylic acid product. This reaction is shown in Figure 3. FTIR, HR-TOF-MS , 1D and 2D NMR spectral analyses were used to elucidate the structure of compound **5**.

The IR spectrum of 22α-carboxyacid-dysobinin (**5**) showed several essential peaks. The vibration frequencies of the O–H hydroxyl, Csp^3–H, and C=O carbonyl groups were identified at 3453 cm^{-1}, 2933 cm^{-1}, and 1744 cm^{-1}, respectively. The peak at 1455 cm^{-1} corresponds to the C=C alkene groups, and the peak at 1247 cm^{-1} is associated with the C–O ether groups. HR-TOF-MS analysis showed that **5** exhibited a molecular ion fragment $[M+H]^+$ at 541.2811 (calcd, 541.2801). A comparison of the NMR spectra of 22α-carboxyacid-dysobinin ($C_{31}H_{40}O_8$) (**1**) and dysobinin ($C_{30}H_{38}O_6$) (**5**) is shown in Table 1. The ^{1}H-NMR spectrum exhibited the presence of seven tertiary methyls, five methyls in the upfield chemical shift (δ_H 0.85, 1.17, 1.19, 1.25, and 1.34, s, 3H), and two methyls tertiary in the downfield chemical shift (δ_H 1.99 and 2.01, each 3H). In addition, the presence of oxymethine protons for H-6 and H-7 at δ_H 5.42 (1H, m) and 5.47 (1H, m), respectively, and three olefinic methine groups at δ_H 5.38 (1H, m), 5.94 (1H, d, J=10.3 Hz), 7.16 (1H, d, J=10.1 Hz), and 7.23 (1H, s) for H-15, H-2, and H-1, respectively, are characteristic of dysobinin [27]. However, in

compound **5**, the furan skeleton has changed, with the addition of one oxymethylen proton at δ_H 4.85 (1H, d, *J*=2.6 Hz) for H-23, one oxymethine proton at δ_H 2.80 (1H, d, *J*=1.8 Hz) for H-22, and one olefinic methine proton at δ_H 7.23 (1H, s), making compound **5** a new, undiscovered compound. Analysis of the ^{13}C-NMR, DEPT-135°, and (HSQC) spectra showed that compound **5** contains thirty-one carbons, representing the addition of one carbon compared to the initial structure of dysobinin. Compound **5** contains four carbonyls for the ketone and ester groups (δ_C 204.6, 170.1, 170.3, and 174.2) and seven methyl tertiary groups (δ_C 20.5, 20.8, 21.0, 21.1, 21.4, 26.9, and 31.7). The ^{13}C NMR spectra also displayed three methylenes (δ_C 16.4, 32.6, and 34.0), one oxymethylene (δ_C 69.9), and four aliphatic methines (δ_C 37.0, 47.9, 50.7, and 50.9). Additionally, there were three methine olefinic (δ_C 119.2, 126.1, and 157.3), two oxymethines (δC 70.2, and 74.6), one oxygenated sp2 methine carbon (δC 146.6), and six quaternary carbons, including sp^3 and sp^2 quaternary carbon (δ_C 40.8, 43.1, 44.9, 47.3, 134.1, and 158.1) [31]. The structural differences between compound **5** and dysobinin include the presence of carbonyl, aliphatic methine, and oxymethylene groups.

The presence of a group bound to **5** is reinforced by the HMBC spectrum (Figure 4), including the position of the ketone and two acetyls in rings A and B. The presence of a carbonyl group at C-3 in ring A was confirmed by the correlations between H-28 (δ_H 1.17) and H-29 (δ_H 1.19) with C-3 (δ_C 204.6). The positions of the acetyl groups at C-6 and C-7 in ring B were confirmed by the correlations between H-6 (δ_H 5.47) and H-7 (δ_H 5.42) with C-1″ (δ_C 170.1) and C-2″ (δ_C 170.3), respectively. The correlation of H-22 (δ_H 2.80) with C-1‴ (δ_C 174.2) prove that the carboxyl group at C-1‴ in the ring dihydrofuran. Furthermore, four cyclic rings were shown from the ^{1}H-^{1}H COSY spectrum, namely the correlation of H-1/H-2 in ring A, H-5/H-6/H-7 in ring B, H-9/H-11/H-12 in ring C, and H-15/H-16/H-17 in ring D. In addition, the ^{1}H-^{1}H COSY correlation between H-22/H-23 and HMBC correlations between H-17 (δ_H 2.83) to C-20 (δ_C 134.1), H-22 (δ_H 2.80) to C-20 (δ_C 134.1) and H -23 (δ_H 4.85) to C-20 (δ_C 134.1), C-21 (δ_C 146.6) confirmed the dihydrofuran ring in compound **5**. The relative configuration of compound **5** was determined using the NOESY spectrum (Figure 5) and comparative NMR data for its analogues [27]. The NOESY spectrum showed a correlation between H-22 (δ_H 2.80) and H-17 (δ_H 2.83), where H-17 is β-oriented, and so H-22 is β-oriented, too, while the carboxyl group attached to C-22 is α-oriented.

3.2. Cytotoxic Activity

All compounds **1**–**5** and doxorubicin, as positive controls, were assessed for cytotoxic activity against breast cancer (MCF-7), cervical cancer (HeLa), melanoma cancer (B16-F10), and normal African green monkey kidney fibroblast cells (CV-1 cells) using a previously described approach [31]-[33]. The experiments were conducted in duplicate, and the data are presented as mean values. According to the IC_{50} values shown in Table 2, compound **5** against MCF-7 cancer cells had the lowest anticancer activity compared to other cancer cell lines. In contrast, compound **5** showed comparatively stronger cytotoxic activity against HeLa and B16-F10 cells, with IC_{50} values of 18.30

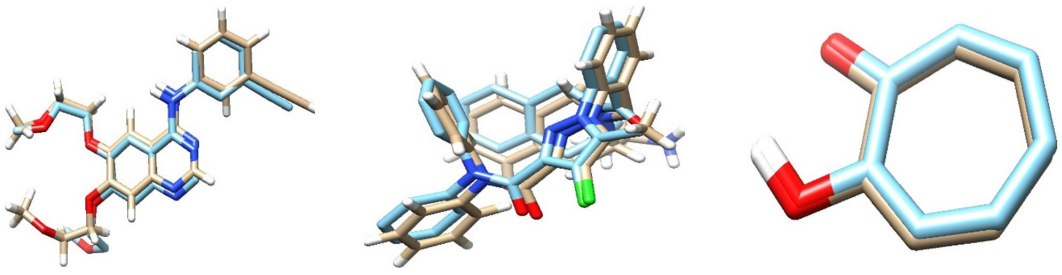

(a) **(b)** **(c)**

Figure 6. Superimposed structures of ligands before docking (white) and after docking (blue): (a) erlotinib, (b) DRO, and (c) tropolone.

Table 3. Docking results of compounds **1**–**5** against EGFR, Bcl-2, and Tyrosinase.

Compound	Protein EGFR		Protein Bcl-2		Protein Tyrosinase	
	Binding Energy (kcal/mol)	H-bond	Binding Energy (kcal/mol)	H-bond	Binding Energy (kcal/mol)	H-bond
1	-8.36	Lys692, Lys704	-7.96	Asn102	-6.90	His244, Asn260
2	-8.25	Lys692, Lys704	-8.02	Arg105	-7.07	Asn260
3	-6.62	Lys692, Lys704, Leu694	-7.16	Arg105	-6.38	Asn81, Arg268, His244
4	-7.97	Lys692, Lys704, Leu694	-7.52	Arg105	-6.94	Glu256, His244
5	-9.61	Lys692, Lys704, Leu694, Met769, Gln767	-7.81	Arg105, Asn102	-6.08	Ser282, Asn260, His244
Erlotinib	-8.21	Lys704, Cys773, Met769	-	-	-	-
DRO	-	-	-10.47	-	-	-
Tropolone	-	-	-	-	-4.63	Ser282, Met280

and 23.84 µg/mL, respectively. These values are within a similar range to those observed for doxorubicin (IC_{50} = 16.24 and 51.85 µg/mL). According to the findings, compound **5** exhibited better anticancer activity against HeLa and B16-F10 than the other compounds. All tested compounds showed little cytotoxicity towards normal CV-1 cells (IC_{50} values >150 µg/mL), indicating a safe profile and selective activity towards cancer cell lines. Selectivity analysis showed that 22α-carboxyacid-dysobinin (**5**) had a significant SI value of 7.43, indicating pronounced selectivity for cancer cells compared to normal CV-1 cells.

Structure–activity relationship (SAR) analysis of compounds **1**–**5** revealed that structural modifications to the limonoid skeleton significantly influenced their cytotoxic activity. Dysobinin (**1**), which retains an intact furan ring, exhibited moderate cytotoxicity against MCF-7, HeLa, and B16-F10 cell lines, suggesting that the furan moiety plays a crucial role in maintaining biological activity owing to its π-electron-rich nature and potential involvement in molecular interactions with biological targets. However, further structural modifications of this moiety led to significant changes in its activity. Compound **5**, in which the furan ring undergoes oxidative cleavage to form a carboxylic acid group, exhibited significantly enhanced cytotoxicity against HeLa and B16-F10 cells. This finding suggests that the introduction of a polar functional group, such as –COOH, enhances binding interactions, likely through hydrogen bonding and electrostatic interactions with cellular targets [34]. Conversely, the presence of an acetoxy group, as observed in 11α-acetoxydysobinin (**2**), significantly decreased the activity across all tested cell lines. This reduction may be attributed to increased steric hindrance and excessive lipophilicity, which negatively affect cellular uptake and target-binding affinity. A similar trend was observed for **4**, where structural modification involving alkoxy substitution led to weak cytotoxic activity. These results indicate that acetylation and alkoxy substitution tend to reduce the biological activity. The presence of hydroxyl groups also influences the biological activity and selectivity. Dysobinol (**3**), which contains an additional hydroxyl group, exhibited moderate and selective activity, particularly against B16-F10 cells.

These observations suggest that hydroxyl groups may facilitate intracellular interactions and redox processes, thereby increasing the oxidative stress. HeLa and B16-F10 cells are highly sensitive to increased ROS levels, which cause mitochondrial damage and trigger apoptosis [35][36]. MCF-7 cells have a relatively more complex antioxidant defence mechanism and are therefore insensitive to ROS [37]. Overall, the SAR trends observed in this study indicate that the oxidation of the furan ring to generate carboxylic acid functionality is the most favourable modification to enhance cytotoxic activity, especially in Hela and B16-F10 cells.

3.3. Molecular Docking Study

A molecular docking study was conducted to identify the potential interactions between compounds **1**-**5** and EGFR, Bcl-2, and tyrosinase. The docking protocol was validated using the root-mean-square deviation (RMSD) parameter. The RMSD is a widely accepted metric for validating docking procedures through redocking analyses, as it ensures the reliability and accuracy of molecular docking outcomes [38]. The RMSD values for erlotinib (0.94 Å), phenyl tetrahydroisoquinoline amide (DRO) (0.90 Å), and tropolone (0.15 Å) were all below the acceptable threshold of 2 Å, indicating that the docking parameters were valid and reliable for compounds **1**–**5**. The superimposed structures of these compounds are shown in Figure 6.

EGFR is a transmembrane receptor tyrosine kinase involved in cell proliferation and survival, and its dysregulation is associated with cancer, including MCF-7 cells [39]. In this study, molecular docking was performed to predict the potential inhibitory mechanisms of compounds with reported anticancer activity against MCF-7 cells. The docking results showed that the binding energies of all compounds 1-5 fall in the range of -6.62 to -9.61 kcal/mol (Table 3). Compared to erlotinib (-8.21 kcal/mol), compounds **1**, **2**, and **5** had lower binding energies, implying that these compounds had better inhibitory activity against the EGFR protein. The 2D interaction analysis revealed that all compounds bound within the EGFR active site, with interaction patterns partially overlapping with those of the native ligand, erlotinib (Figure 7). Erlotinib formed key hydrogen bond interactions with residues such as Lys704, Cys773, and Met769, along with hydrophobic contacts (alkyl and π-alkyl) with Val702, Lys721, and Leu768, respectively. The π-

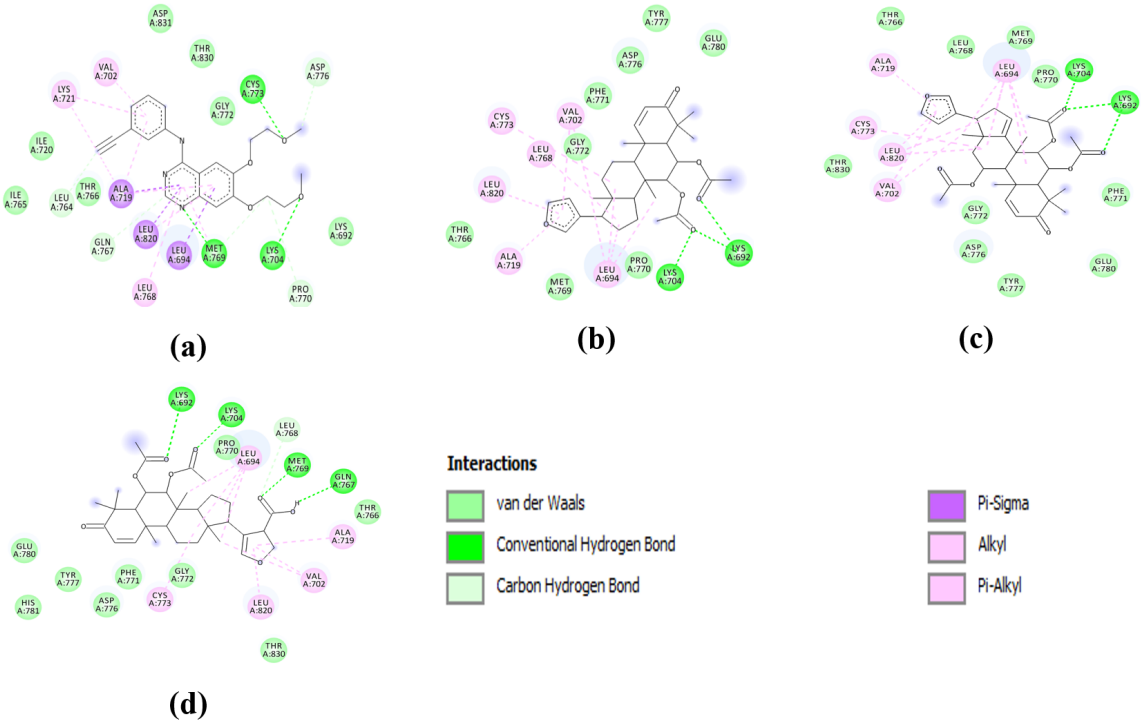

Figure 7. 2D-Intermolecular interactions of (a) erlotinib, as well as (b) compounds **1**, (c) **2**, and (d) **5**, in the active site of the EGFR protein.

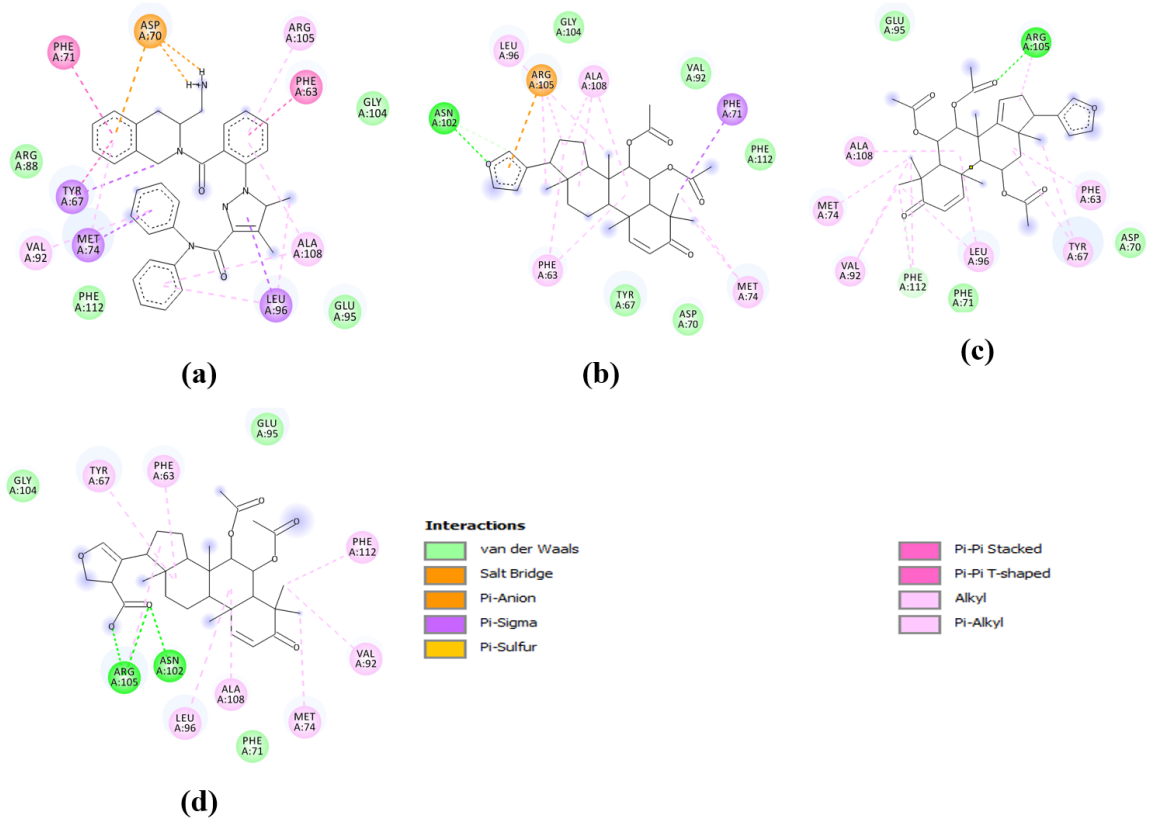

Figure 8. 2D-Intermolecular interactions of (a) DRO, as well as (b) compounds **1**, (c) **2**, and (d) **5** in the active site of Bcl-2 protein.

sigma interactions are formed with amino acid residues Leu694, Ala719, and Leu820, which are essential for stable binding within the active site. Compounds **1** and **2** exhibited similar interaction profiles, including hydrogen bonding with Lys704 and hydrophobic interactions with surrounding residues, suggesting a binding mode comparable to that of erlotinib. In contrast, compound **5** showed multiple hydrophobic interactions and hydrogen bonding with Lys692, Lys704, Gln767, and Met769, indicating a strong binding affinity, as reflected by its favourable docking score. However, no direct correlation was observed between the docking scores and cytotoxic activity against MCF-7 cells. Compound **5** showed the most favorable binding energy but weak activity (IC_{50} > 300 µg/mL), whereas compound **1** exhibited the strongest activity (IC_{50} = 66.7 µg/mL) despite a less favorable docking score. These results indicate that docking provides only a preliminary estimate of binding affinity and does not directly predict biological activity, as factors such as cell permeability may influence the observed in vitro effects of the compounds.

Molecular docking studies of compounds **1**–**5** were also performed against the Bcl-2 protein. The docking results showed that compounds **1**–**5** exhibited binding energies ranging from −7.16 to −8.02 kcal/mol, which were less favourable than that of the native ligand DRO (−10.47 kcal/mol). Compound **2** displayed the lowest binding energy (−8.02 kcal/mol), followed by compounds **1** (−7.96 kcal/mol) and **5** (−7.81 kcal/mol), respectively. Furthermore, 2D interaction analysis demonstrated that compounds **1**, **2**, and **5** bind within the Bcl-2 active site through a combination of hydrogen bonding, hydrophobic, π-related, and electrostatic interactions (Figure 8). The native ligand DRO exhibits diverse interactions, including π–π stacking, π–anion, and hydrophobic (alkyl and π–alkyl) contacts with key residues such as Phe63, Tyr67, and Arg105, which contribute to stable binding of the ligand. Compounds **1** and **2** show similar interaction patterns, forming π–π and π–alkyl interactions with aromatic residues (e.g., Phe63 and Tyr67), along with hydrophobic contacts

and limited electrostatic contributions. Hydrogen bonds were also observed between Asn102 and Arg105. In contrast, compound **5** exhibited a more diverse interaction profile, including hydrogen bonds with Arg105 and Asn102, which may enhance the binding stability within the active site. These interaction patterns are consistent with *in vitro* results, where compound **5** demonstrated stronger cytotoxic activity against HeLa cells than compounds **1** and **2**.

The docking results against tyrosinase showed that compounds **1**–**5** exhibited binding energies ranging from −6.08 to −7.07 kcal/mol, which were more favorable than those of the native ligand tropolone (−4.63 kcal/mol). Compound **2** displayed the lowest binding energy (−7.07 kcal/mol), followed by compounds **4** and **1**, respectively. The 2D interaction analysis indicated that the ligands bind within the tyrosinase active site through a combination of hydrogen bonding, hydrophobic, and π-related interactions (Figure 9). The native ligand, tropolone, forms key hydrogen bonds and hydrophobic interactions with residues such as Met280 and Ser282, which are important for stabilizing the binding within the active site. Another study found that tropolone forms hydrogen bonds with the Asn260 residue [40]. Compound **5** exhibited a more extensive interaction profile, including multiple hydrogen bonds with residues such as His244, Asn260, and Ser282, which may enhance binding stability. In addition, compound **5** formed π–sigma and π–alkyl interactions with residues such as His263 and Val283, along with van der Waals contacts that supported its accommodation within the binding pocket. Compounds **1** and **3** also demonstrate hydrogen bonding and hydrophobic interactions; however, their interaction networks are less extensive compared to compound **5**, particularly in terms of π -related interactions and the number of hydrogen bonds. This is consistent with the stronger cytotoxic activity against B16-F10 cells, although the correlation remains limited because docking primarily reflects binding affinity and does not fully account for biological factors such as cell permeability and intracellular mechanisms.

3.4. Physicochemical and ADMET Properties

The pharmacokinetic properties of compound **5** were obtained from the pkCSM website. The physicochemical properties of drug candidates should have the following characteristics: logarithm

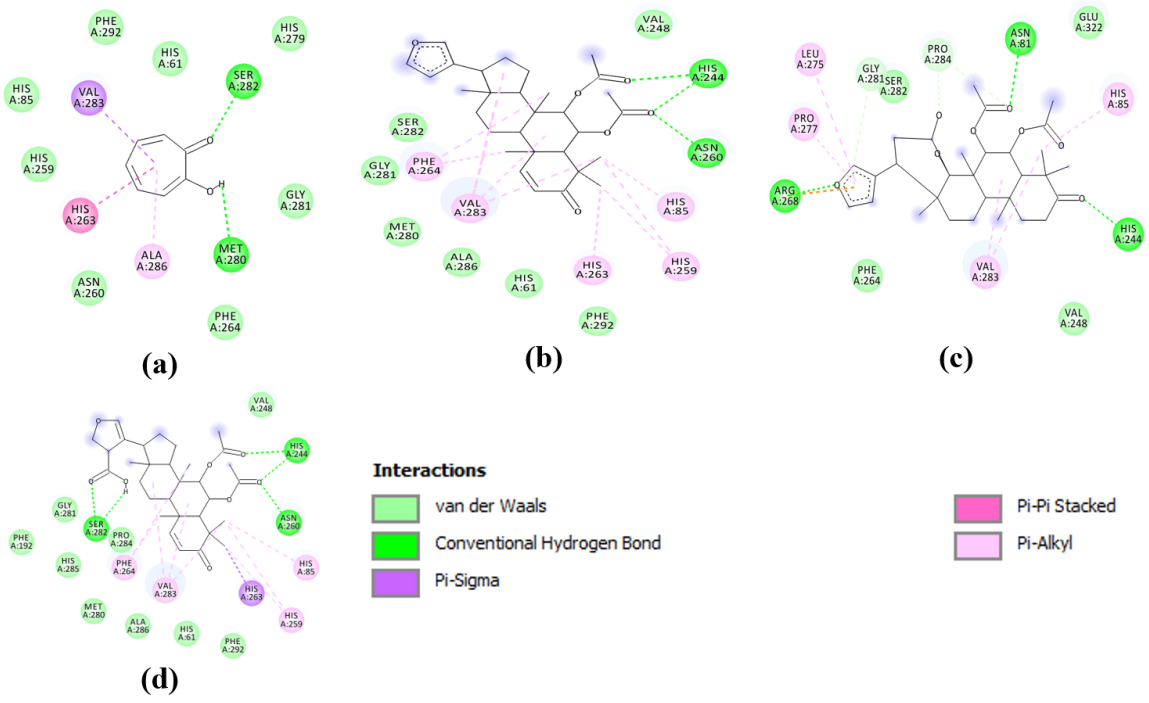

Figure 9. 2D-Intermolecular interactions of (a) tropolone, as well as (b) compounds **1**, (c) **2**, and (d) **5** in the active site of tyrosinase protein.

Table 4. Physicochemical and ADMET properties of compound **5**.

	Properties	Compound 5
Physicochemical	Molecular weight	540.653
	log P	4.634
	Rotatable bond	4
	H-bond acceptor	7
	H-bond donor	1
	Surface area	229.371
Absorption	Caco-2 permeability	1.416
	Intestinal absorption	79.027
	Skin permeability	-2.946
Distribution	VDss	-0.338
	BBB permeability	-0.846
	CNS permeability	-3.007
Metabolism	CYP2D6 substrate	No
	CYP3A4 substrate	Yes
	CYP2D6 inhibitor	No
	CYP3A4 inhibitor	No
Excretion	Total clearance	-0.048
	Renal OCT2 substrate	No
Toxicity	AMES Toxicity	No
	Max. Tolerated dose	-0.865
	hERG I inhibitor	No
	hERG II inhibitor	No
	Hepatoxicity	No
	Skin sensitization	No

of the octanol-water partition coefficient (log P) <5, molecular weight <500 Da, polar surface area (PSA) <140 Å, hydrogen bond acceptor (HBA) <10, hydrogen bond donor (HBD) <5, and rotatable bonds (ROTB) <10, according to Lipinski's rule of five [41]. As shown in Table 4, compound **5** did not fulfil the molecular weight or polar surface area parameters for the predicted pKa. ADMET properties are important for drug development, particularly for determining the ability of small-molecule medications to metabolize, distribute, absorb, excrete, and be toxicologically. The Caco-2 model is a common in vitro tool for estimating human intestinal absorption and predicting oral drug uptake in humans. A compound is considered highly permeable when its Caco-2 value is 0.90 [42]. Compound **5** exceeded this threshold value. IA reflects the amount of drug absorbed by the human intestine. An absorption rate of 80% is regarded as good, and a rate lower than 30% is considered unfavourable [43]. The IA value of compound 5 was 79.027%, implying that compound **5** was easily absorbed by the human intestine.

The distribution of compound **5** was determined using the volume distribution (VDss). The VDss parameter represents the overall amount of the substance in the body and has a low value (log VDss < -0.15) [44]. The VDss value of compound **5** was less than -0.15, indicating a lower distribution in the tissue than in the plasma. Subsequently, BBB permeability describes how drugs pass through the blood-brain barrier. A drug candidate with a logBB of more than 0.3 is easily absorbed into the brain [45]. Assessment of central nervous system (CNS)

permeability is another approach for evaluating blood-brain barrier penetration. A LogPS value greater than –2 indicates potential absorption into the CNS, whereas a value below –3 suggests an inability to reach the CNS. Based on BBB and CNS metrics, compound **5** exhibited moderate capacity to permeate the blood-brain barrier but was not absorbed into the CNS.

Compound **5** was more likely to serve as a CYP3A4 substrate than as a CYP2D6 substrate and did not exhibit any inhibitory activity towards these substrates. Cytochrome P450 (CYP) metabolism is highly dependent on these enzymes and is an essential detoxifying enzyme found mainly in the human liver. Furthermore, the excretion parameters showed that compound **5** had a total clearance value of -0.048 and did not comply with Renal Organic Cation Transporter 2 (OCT2), and the OCT2 parameter indicates the removal and clearance of drugs. Toxicity parameters suggested that compound 5 had no mutagenic potential, according to the AMES toxicity test. The maximum tolerated dose (MTD) is defined as the upper limit of safe exposure to a substance in humans. The MRTD values indicated low toxicity for compound **5**, which showed no inhibitory activity against hERG I or II. hERG-induced potassium channel blockage can trigger long-QT syndrome, causing fatal ventricular arrhythmia. The final toxicity parameters were determined based on hepatotoxicity and skin sensitization. The results showed that compound **5** did not affect the liver or skin.

4. CONCLUSIONS

In conclusion, dysobinin (**1**) was successfully treated with Selectfluor to form 22α-carboxyacid-dysobinin (**5**) in 56% yield. Cytotoxicity assays revealed that compound **5** exhibited the most potent anticancer activity, with IC_{50} values of 18.30 and 23.84 µg/mL against HeLa and B16-F10 cancer cells, respectively. Subsequently, a docking study showed that compound **5** had binding energies of -9.61, -7.81, and -6.08 kcal/mol for EGFR, Bcl-2, and tyrosinase, respectively. ADMET prediction indicated that compound **5** possesses several favorable pharmacokinetic and toxicity-related properties; however, it did not fully comply with conventional drug-likeness criteria. Therefore, compound **5** may be considered a promising lead compound for anticancer development, warranting further optimization and validation.

AUTHOR INFORMATION

Corresponding Author

Nurlelasari Nurlelasari — Department of Chemistry, Universitas Padjadjaran, Jatinangor-45363 (Indonesia);

orcid.org/0000-0002-9317-2607

Email: nurlelasari@unpad.ac.id

Authors

Muhammad Badrul Huda — Department of Chemistry, Universitas Padjadjaran, Jatinangor-45363 (Indonesia); Department of Chemistry, Universitas Diponegoro, Semarang-50275 (Indonesia);

orcid.org/0009-0003-0464-5543

Faris Hermawan — Research Center for Pharmaceutical Ingredients and Traditional Medicine, National Research and Innovation Agency (BRIN), Cibinong-16911 (Indonesia);

orcid.org/ 0009-0006-6923-4050

Wahyu Safriansyah — Eijkman Research Center for Molecular Biology, National Research and Innovation Agency (BRIN), Cibinong-16911 (Indonesia);

orcid.org/ 0000-0002-3243-4001

Unang Supratman — Department of Chemistry, Universitas Padjadjaran, Jatinangor-45363 (Indonesia); Central Laboratory, Universitas Padjadjaran, Jatinangor-45363 (Indonesia);

orcid.org/0000-0002-1104-2321

Yudha Prawira Budiman — Department of Chemistry, Universitas Padjadjaran, Jatinangor-45363 (Indonesia);

orcid.org/0000-0002-3929-1891

Author Contributions

Conceptualization was carried out by M. B. H. and U. S. Methodology was developed by M. B. H., N. N., and W. S. Software and computational analysis were performed by Y. P. B. Validation of chemical and biological data was conducted by M. B. H., N. N., and U. S. Formal analysis was

completed by M. B. H. and Y. P. B. Investigation including isolation, synthesis, and cytotoxicity studies was conducted by M. B. H., W. S., and F. H. Resources were provided by U. S. and N. N. Data curation was performed by M. B. H. and F. H. Writing – original draft preparation and project administration was handled by M. B. H., while writing – review and editing were performed by N. N., U. S., and Y. P. B. Visualization was conducted by Y. P. B. Supervision was provided by N. N. and U. S. Funding acquisition was secured by U. S.

Conflicts of Interest

The authors declare no conflict of interest.

ACKNOWLEDGEMENT

The Ministry of Education, Culture, Research, and Technology in Indonesia provided financial support for this study through a Doctoral Research Grant (Grant Recipient: NS, No: 3966/UN.6.3.1/PT.00/2024) and a Fundamental Grant (Grant Recipient: NS, No: 3965/UN6.3.1/PT.00/2024).

DECLARATION OF GENERATIVE AI

Not applicable.

REFERENCES

[1] R. L. Siegel, K. D. Miller, N. S. Wagle, and A. Jemal. (2023). "Cancer statistics, 2023". *CA: A Cancer Journal for Clinicians.* **73** (1): 17-48. 10.3322/caac.21763.

[2] F. Bray, M. Laversanne, H. Sung, J. Ferlay, R. L. Siegel, I. Soerjomataram, and A. Jemal. (2024). "Global Cancer Statistics 2022: GLOBOCAN Estimates of Incidence and Mortality Worldwide for 36 Cancers in 185 Countries". *CA: A Cancer Journal for Clinicians.* **74** : 229-263. 10.3322/caac.21834.

[3] C. B. Blackadar. (2016). "Historical Review of the Causes of Cancer". *World Journal of Clinical Oncology.* **7** (1): 54-86. 10.5306/wjco.v7.i1.54.

[4] M. P. Crespo-Ortiz and M. Q. Wei. (2012). "Antitumor Activity of Artemisinin and Its Derivatives: From a Well-Known Antimalarial Agent to a Potential Anticancer Drug". *Journal of Biomedicine and Biotechnology.* **2012** : 247597. 10.1155/2012/247597.

[5] G. Danaei, S. Vander Hoorn, A. D. Lopez, C. J. L. Murray, and M. Ezzati. (2005). "Causes of Cancer in the World: Comparative Risk Assessment of Nine Behavioural and Environmental Risk Factors". *The Lancet.* **366** : 1784-1793. 10.1016/S0140-6736(05)67725-2.

[6] Q. Li, Z. Shi, F. Zhang, W. Zeng, D. Zhu, and L. Mei. (2022). "Symphony of Nanomaterials and Immunotherapy Based on the Cancer-Immunity Cycle". *Acta Pharmaceutica Sinica B.* **12** : 107-134. 10.1016/j.apsb.2021.05.031.

[7] U. Supratman, Supriatno, W. Naibaho, M. Fajar, Nurlelasari, D. G. Katja, D. Harneti, R. Maharani, A. T. Hidayat, R. Lesmana, M. A. Nafiah, and Y. Shiono. (2020). "New Cytotoxic Limonoids from the Stem Bark of Chisocheton pentandrus (Blanco) Merr". *Phytochemistry Letters.* **35** : 63-67. 10.1016/j.phytol.2019.11.002.

[8] Nurlelasari, I. Rahmayanti, S. Salam, A. Safari, D. Harneti, R. Maharani, A. T. Hidayat, M. Tanjung, R. Retnowati, Y. Shiono, and U. Supratman. (2021). "A New Havanensin-Type Limonoid from Chisocheton macrophyllus". *Applied Biological Chemistry.* **64** (1): 1-6. 10.1186/s13765-021-00606-5.

[9] E. Hilmayanti, Nurlelasari, D. G. Katja, A. T. Hidayat, S. Fajriah, A. Darmawan, U. Supratman, M. N. Azmi, and Y. Shiono. (2022). "Azadirone-Type Limonoids from the Fruit of Chisocheton lasiocarpus and Their Cytotoxic Activity Against MCF-7 Breast Cancer Cells". *Molekul.* **17** (1): 60-67. 10.20884/1.jm.2022.17.1.5593.

[10] S. L. Chong, A. Hematpoor, Hazni, M. S. Azirun, M. Litaudon, U. Supratman, M. Murata, and K. Awang. (2019). "Mosquito Larvicidal Limonoids from the Fruits of Chisocheton erythrocarpus Hiern". *Phytochemistry Letters.* **30** : 69-73. 10.1016/j.phytol.2018.12.013.

[11] Nurlelasari, L. W. Azzahra, W. Safriansyah, M. B. Huda, Rustaman, D. Harneti, T. Mayanti, K. Farabi, R. Maharani, and U. Supratman. (2026). "11α-Hydroxydysobinin: A New Limonoid from Chisocheton macrophyllus Seeds (Meliaceae)". *Journal of Asian Natural Products Research.* **28** : 635-642. 10.1080/10286020.2025.2525332.

[12] M. B. Mukesh and K. Rakesh. (2011). "Molecular Docking: A Review". *International Journal of Ayurveda and Pharmacy.* **2** (6): 1746-1750.

[13] C. Sha and P. C. Lee. (2024). "EGFR-Targeted Therapies: A Literature Review". *Journal of Clinical Medicine.* **13** : 6391. 10.3390/jcm13216391.

[14] A. Hawash. (2024). "Targeting EGFR Signaling in Cancer: Mechanisms and Therapeutic Strategies". *Cells.* **13** (19): 1656. 10.3390/cells13191656.

[15] A. Ayati, S. Moghimi, S. Salarinejad, M. Safavi, B. Pouramiri, and A. Foroumadi. (2020). "A Review on Progression of Epidermal Growth Factor Receptor (EGFR) Inhibitors as an Efficient Approach in Cancer Therapy". *Bioorganic Chemistry.* **99** : 103811. 10.1016/j.bioorg.2020.103811.

[16] G. Zhao, W. Wang, L. Zheng, L. Chen, G. Duan, R. Chang, Z. Chen, S. Zhang, M. Dai, and G. Yang. (2023). "Catalase-Peroxidase StKatG Is a Bacterial Manganese Oxidase from Endophytic Salinicola tamaricis". *International Journal of Biological Macromolecules.* **224** : 281-291. 10.1016/j.ijbiomac.2022.10.123.

[17] M. Chatatikun, T. Yamauchi, K. Yamasaki, and S. Aiba. (2018). "Anti-Melanogenic Effect of Croton roxburghii and Croton sublyratus Leaves in α-MSH-Stimulated B16F10 Cells". *Journal of Traditional Chinese Medical Sciences.* **5** : 1-7. 10.1016/j.jtcme.2017.12.002.

[18] Y. H. Cho, J. E. Park, D. S. Lim, and J. S. Lee. (2017). "Tranexamic Acid Inhibits Melanogenesis by Activating the Autophagy System in Cultured Melanoma Cells". *Journal of Dermatological Science.* **88** (1): 96-102. 10.1016/j.jdermsci.2017.05.019.

[19] R. Jiang, X. H. Xu, and K. Wang. (2017). "Ethyl Acetate Extract from Panax ginseng C.A. Meyer and Its Main Constituents Inhibit α-Melanocyte-Stimulating Hormone-Induced Melanogenesis by Suppressing Oxidative Stress in B16 Mouse Melanoma Cells". *Journal of Ethnopharmacology.* **208** : 149-156. 10.1016/j.jep.2017.07.004.

[20] T. Pillaiyar, M. Manickam, and S. H. Jung. (2017). "Recent Development of Signaling Pathway Inhibitors of Melanogenesis". *Cell Signalling.* **40** : 99-115. 10.1016/j.cellsig.2017.09.004.

[21] D. W. Robbins and J. F. Hartwig. (2012). "A C-H Borylation Approach to Suzuki-Miyaura Coupling of Typically Unstable 2-Heteroaryl and Polyfluorophenyl Boronates". *Organic Letters.* **14** (16): 4266-4269. 10.1021/ol301570t.

[22] M. B. Huda, Nurlelasari, W. Safriansyah, M. Fajar, I. I. Widiyowati, U. Supratman, Y. Permana, and Y. P. Budiman. (2024). "One-Pot Two-Step Borylation/Fluorination Reaction of Dysobinin from Chisocheton macrophyllus and Its Cytotoxicity Against Cancer Cells". *Communications in Science and Technology.* **9** : 366-371. 10.21924/cst.9.2.2024.1514.

[23] E. F. Pettersen, T. D. Goddard, C. C. Huang, G. S. Couch, D. M. Greenblatt, E. C. Meng, and T. E. Ferrin. (2004). "UCSF Chimera: A Visualization System for Exploratory Research and Analysis". *Journal of Computational Chemistry.* **25** (13): 1605-1612. 10.1002/jcc.20084.

[24] M. D. Hanwell, D. E. Curtis, D. C. Lonie, T. Vandermeersch, E. Zurek, and G. R. Hutchison. (2012). "Avogadro: An Advanced Semantic Chemical Editor, Visualization, and Analysis Platform". *Journal of Cheminformatics.* **4** : 17. 10.1186/1758-2946-4-17.

[25] F. Neese. (2012). "The ORCA Program System". *Wiley Interdisciplinary Reviews: Computational Molecular Science.* **2** (1): 73-78. 10.1002/wcms.81.

[26] D. E. V. Pires, T. L. Blundell, and D. B. Ascher. (2015). "pkCSM: Predicting Small-Molecule Pharmacokinetic and Toxicity

Properties Using Graph-Based Signatures". *Journal of Medicinal Chemistry.* **58** (9): 4066 -4072. 10.1021/acs.jmedchem.5b00104.

[27] Nurlelasari, M. B. Huda, W. Safriansyah, U. Supratman, Y. P. Budiman, D. H. P. Huspa, R. Maharani, T. Mayanti, K. Farabi, and S. Fajriah. (2024). "A Novel Limonoid from the Seeds of Chisocheton macrophyllus". *Records of Natural Products.* **18** (3): 347-351. 10.25135/rnp.451.2311.2960.

[28] G. Isabelle, I. Dondasse, C. Nicolas, L. Mimoun, V. Sukach, and H. Meudal. (2022). "Iridium-Catalyzed β-C(sp2)-H Borylation of Enamides: Access to 3,3-Dihalogeno-2-Methoxypiperidines". *European Journal of Organic Chemistry.* **2022** (2). 10.1002/ejoc.202101302.

[29] S. J. Blank and C. E. Stephens. (2006). "Oxidative Ring Opening of 2,5-Diarylfurans by Selectfluor". *Tetrahedron Letters.* **47** (38): 6849-6850. 10.1016/j.tetlet.2006.07.071.

[30] H. Wang, S. Ren, J. Zhang, W. Zhang, and Y. Liu. (2015). "Selectfluor-Mediated Simultaneous Cleavage of C-O and C-C Bonds in α,β-Epoxy Ketones Under Transition-Metal-Free Conditions: A Route to 1,2-Diketones". *Journal of Organic Chemistry.* **80** (13): 6856-6863. 10.1021/acs.joc.5b00857.

[31] Y. L. Zhang, C. C. Chiang, Y. T. Lee, Z. H. Wen, Y. C. Wu, Y. J. Wu, T. L. Hwang, T. Y. Wu, C. Y. Chang, and P. J. Sung. (2020). "Briarenols Q-T: Briaranes from A Cultured Octocoral Briareum stechei (Kukenthal, 1908)". *Marine Drugs.* **18** (8). 10.3390/md18080383.

[32] W. Safriansyah, F. F. Abdullah, E. Juliansyah, K. Farabi, Harizon, H. Kuncoro, Nurlelasari, R. Maharani, M. N. A. Mohamad Taib, U. Supratman, and D. Harneti. (2023). "Sesquiterpenoids from the Stem Bark of Aglaia pachyphylla Miq (Meliaceae) and Cytotoxic Activity Against MCF-7 Cancer Cell Line". *Jurnal Kimia Valensi.* **9** (2): 300-305. 10.15408/jkv.v9i2.32782.

[33] S. Supriatno, Nurlelasari, T. Herlina, D. Harneti, R. Maharani, A. T. Hidayat, T. Mayanti, U. Supratman, M. N. Azmi, and Y. Shiono. (2018). "A New Limonoid from the Stem Bark of Chisocheton pentandrus (Meliaceae)". *Natural Product Research.* **32** : 1-7. 10.1080/14786419.2018.1428600.

[34] Q. Wang, B. Kou, J. Wang, H. Song, J. Gao, Y. Sun, L. Wang, and X. Jin. (2025). "Limonoids and Semisynthetic Derivatives as Anticancer Agents: Recent Research Progress and Future Perspectives". *Bioorganic Chemistry.* **161** : 108520. 10.1016/j.bioorg.2025.108520.

[35] X. Z. Wang, H. H. Yang, W. Li, B. J. Han, and Y. J. Liu. (2016). "Studies on Apoptosis in HeLa Cells via the ROS-Mediated Mitochondrial Pathway Induced by New Dibenzoxanthenes". *New Journal of Chemistry.* **40** (6): 5255-5267. 10.1039/C6NJ00250A.

[36] M. Jopp, J. Becker, S. Becker, A. Miska, V. Gandin, C. Marzano, and S. Schindler. (2017). "Anticancer Activity of a Series of Copper(II) Complexes with Tripodal Ligands". *European Journal of Medicinal Chemistry.* **132** : 274-281. 10.1016/j.ejmech.2017.03.019.

[37] A. C. Martínez-Torres, A. Reyes-Ruiz, K. M. Calvillo-Rodriguez, K. M. Alvarez-Valadez, A. C. Uscanga-Palomeque, R. S. Tamez-Guerra, and C. Rodríguez-Padilla. (2020). "IMMUNEPOTENT CRP Induces DAMPs Release and ROS-Dependent Autophagosome Formation in HeLa and MCF-7 Cells". *BMC Cancer.* **20** : 647. 10.1186/s12885-020-07124-5.

[38] J. Eberhardt, D. Santos-Martins, A. F. Tillack, and S. Forli. (2021). "AutoDock Vina 1.2.0: New Docking Methods, Expanded Force Field, and Python Bindings". *Journal of Chemical Information and Modeling.* **61** (8): 3891-3898. 10.1021/acs.jcim.1c00203.

[39] Y. S. Kwon, K. S. Nam, and S. Kim. (2021). "Tamoxifen Overcomes Trastuzumab Resistance of SK-BR-3 Tumourspheres by Targeting Crosstalk Between Cytoplasmic Estrogen Receptor α and the EGFR/HER2 Signaling Pathway". *Biochemical Pharmacology.* **190** : 114635. 10.1016/j.bcp.2021.114635.

[40] P. Zhou, J. Hu, X. Wang, J. Wang, Y. Zhang, and C. Wang. (2018). "Epidermal Growth Factor Receptor Expression Affects Proliferation and Apoptosis in Non-Small Cell Lung Cancer Cells via the Extracellular Signal-Regulated Kinase/MicroRNA-200a Signaling Pathway". *Oncology Letters.* **15** : 5201-5207. 10.3892/ol.2018.7961.

[41] C. Pan, X. Li, Y. Zhang, Z. Zhang, Y. Li, B. Chen, G. Li, L. Zhang, C. Deng, H. A. Akber, Z. Du, and Z. Yang. (2023). "The Mechanisms of Melanogenesis Inhibition by Glabridin: Molecular Docking, PKA/MITF and MAPK/MITF Pathways". *Food Science and Human Wellness.* **12** (1): 212-222. 10.1016/j.fshw.2022.07.011.

[42] T. K. Karami, S. Hailu, S. Feng, R. Graham, and H. J. Gukasyan. (2022). "Eyes on Lipinski's Rule of Five: A New Rule of Thumb for Physicochemical Design Space of Ophthalmic Drugs". *Journal of Ocular Pharmacology and Therapeutics.* **38** (1): 1-9. 10.1089/jop.2021.0069.

[43] Y. Wang, M. Yu, A. T. Amrouche, F. Jie, S. Ji, and B. Lu. (2023). "Human Intestinal Caco-2 Cell Model to Evaluate the Absorption of Bioactive Compounds and Their Effects on Transport Mechanisms". *Food Science and Human Wellness.* **12** (5): 1701-1707. 10.1016/j.fshw.2023.02.032.

[44] E. Radchenko, A. Dyabina, V. Palyulin, and N. Zefirov. (2016). "Prediction of Human Intestinal Absorption of Drug Compounds". *Russian Chemical Bulletin.* **65** : 576-580. 10.1007/s11172-016-1340-0.

[45] N. Flores-Holguin, J. Frau, and D. Glossman-Mitnik. (2021). "Computational Pharmacokinetics Report, ADMET Study, and Conceptual DFT-Based Estimation of the Chemical Reactivity Properties of Marine Cyclopeptides". *ChemistryOpen.* **10** (11): 1142-1149. 10.1002/open.202100178.